The freezing behavior of aqueous *n*-alcohol nanodroplets

Tong Sun[a], Dor Ben-Amotz,[b] Barbara E. Wyslouzil*[ac]

[a] William G. Lowrie Department of Chemical and Biomolecular Engineering, The Ohio State University, Columbus, OH 43210, USA.

[b] Department of Chemistry, Purdue University, West Lafayette, IN 47907, USA

[c] Department of Chemistry and Biochemistry, The Ohio State University, Columbus, OH 43210, USA.

I. Partitioning Calculations

The surface tension of the droplet $\sigma(x^b, T)$ is assumed to be a function of its bulk mole fraction x^b and temperature. For a given choice of x^b, the surface composition is determined by assuming the surface tension is equal to the molecular volume fraction weighted average of each component in the surface monolayer as:

$$\sigma(x^b, T) = \frac{\sigma_1 v_1 x_1^s + \sigma_2 v_2 x_2^s}{v_1 x_1^s + v_2 x_2^s}. \quad \text{(S.1)}$$

Here 1 and 2 denote water and alcohol, respectively, and v_i and σ_i are the molecular volume and surface tension of each pure component. The average thickness δ of the monolayer is then calculated as:

$$\delta = \left(\frac{6}{\pi}(v_1 x_1^s + v_2 x_2^s)\right)^{\frac{1}{3}}, \quad \text{(S.2)}$$

corresponding to a surface volume V_s given by

$$V_s = \frac{4\pi}{3}[r^3 - (r-\delta)^3]. \quad \text{(S.3)}$$

The surface phase must also satisfy mass balance:

$$n_1^s m_1 + n_2^s m_2 = \rho(x^s) V_s, \quad \text{(S.4)}$$

where n_i and m_i represent the moles and molecular weight of each species, respectively. The density of the surface phase ρ as a function of the monolayer composition can be calculated as:

$$\rho(x^s) = \frac{m_1 x_1^s + m_2 x_2^s}{v_1 x_1^s + v_2 x_2^s}. \quad \text{(S.5)}$$

The partitioning calculation is performed iteratively while ensuring the constraints that $x_1^s + x_2^s = 1$ and $x_1^b + x_2^b = 1$. The density data for each component and the deviation of density from the ideal system are listed in Physical Properties section in the Supporting Information.

$\sigma(x^b, T)$ is determined by first extrapolating temperature dependent surface tension data measured in bulk aqueous mixtures at fixed compositions of *n*-propanol[1] and *n*-pentanol[2], to 220 K. These values are then fit to the Szyszkowski equation to obtain the empirical parameters A and B:

$$\sigma(T) = \sigma_w(T) - A\ln(1 + \frac{C_b}{B}), \tag{S.6}$$

where σ_w is the surface tension of water and C_b is the molarity of the solute in the bulk phase or total molarity in a bulk system. The surface tensions of 1-pentanol were measured below the solubility limit ($x_2 < 0.0031$) in the temperature range of 25-85 °C. As demonstrated in the results, even when the total mole fraction of alcohol in the aerosol is above this limit, the model suggests the bulk concentration is still well below the limit.

II. Nozzle Profile

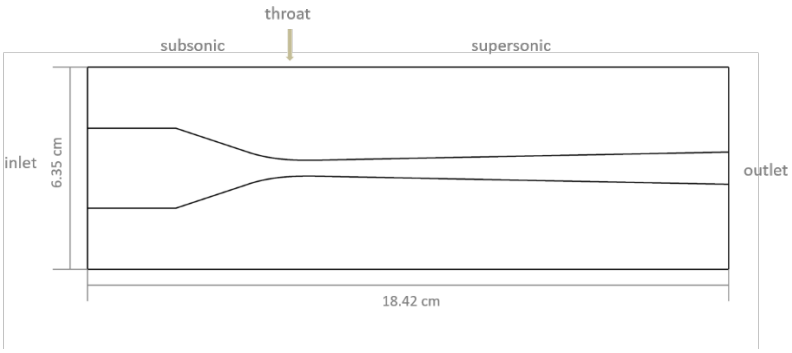

Fig. S1 The design of the converging-diverging supersonic nozzle profile incorporates shaped upper and lower blocks and flat sidewalls separated by 1.27 cm. The throat height is 0.50 cm and 1.27 cm, respectively. The height at the entrance is 2.51 cm and at the outlet is 1.01 cm.

III. Pressure Trace Measurements

A. Full Measurement Results

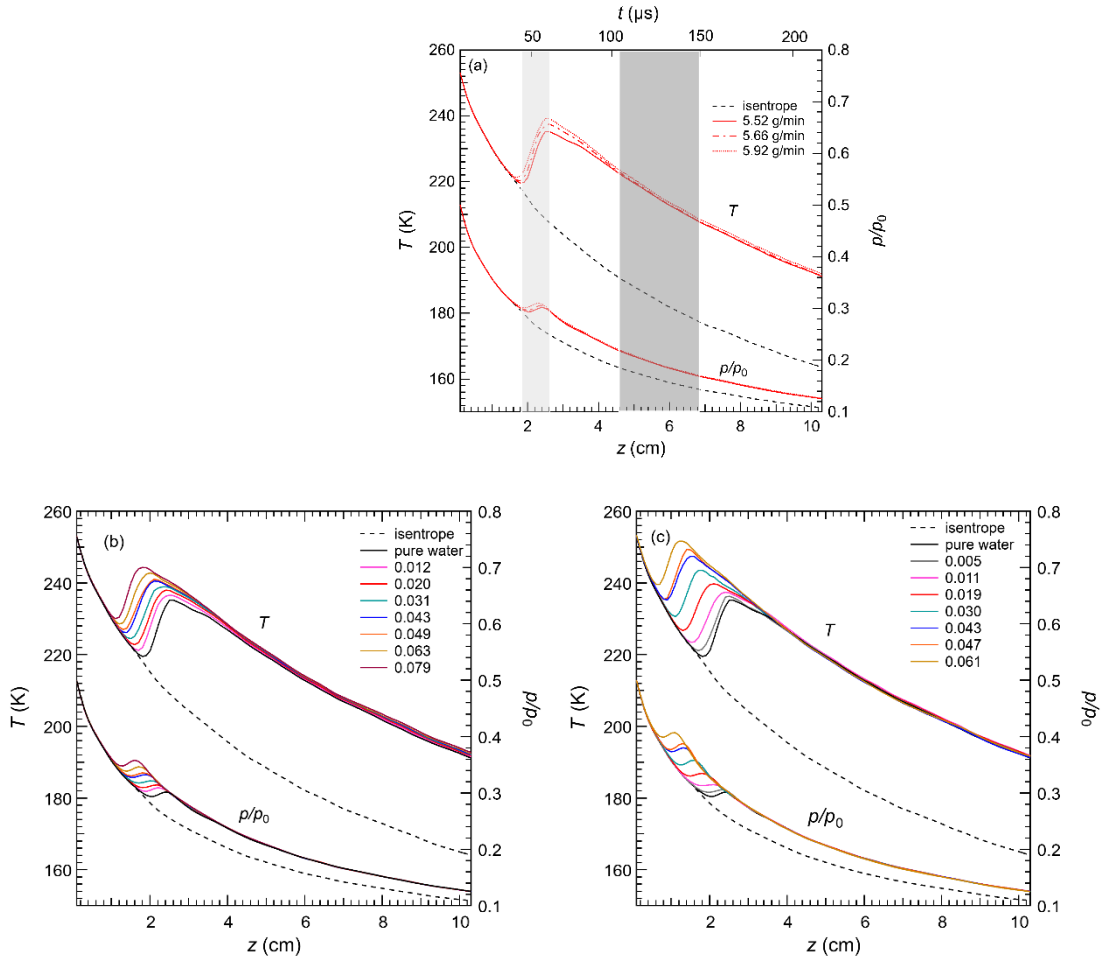

Fig. S2 (a) Pure water temperature and pressure ratio profiles from PTM for the mass flow rates of water indicated, where 5.52 g/min corresponds to the base case used in all of the n-alcohol experiments. Even with an extra 0.4 g/min of water, corresponding to an extra 0.068 mol H_2O/min relative to the base case, condensation is only shifted upstream by ~0.1 cm. The light gray and dark gray shaded area indicate the regions of rapid condensation and freezing, respectively. (b) Full pressure traces for water with propanol, and (c) water with pentanol.

B. Overall Composition of the Condensate

In this paper we assume that by the time we observe freezing enough of the incoming material has condensed that the composition of the aerosol is the same as that of the incoming vapor. To demonstrate that this is a reasonable assumption we considered the case for the highest concentration of 1-propanol. At the inlet to the nozzle this corresponds to $y_{H2O,0} = 1.61\times10^{-2}$ and

$y_{1\text{-prop},0} = 1.09\times10^{-3}$.

To start, we assume the droplet composition equals that of the initial vapor and calculate the partial pressure of each species above the highly curved 6 nm nanodroplet and T = 220 K (just prior to freezing) using the following equations,

$$p_i = x_i^b \gamma_i p_{eq,i} \exp\frac{2\sigma v_i}{r k_B T} \quad \text{(S.7)}$$

where γ_i is the activity coefficient of species i in the mixed droplet, x_i^b and σ are based on the Malila and Priesle model. For these water rich droplets we can we assume $\gamma_1 = 1$. For 1-propanol, we used the correlation for the temperature dependence of the activity coefficient $\gamma_2^\infty(T)$ at infinite dilution developed by Donhal *et al.*[3] as an upper bound for γ_2 in our temperature range,

$$\gamma_2^\infty(T) = -2.5530 + (8.6101/\tau) - (52.3154/\tau)\exp[-2.7321\tau] \quad \text{(S.8)}$$

where $\tau = T/T_0$ and T_0 = 298.15 K. The sharp decrease in $\gamma_2^\infty(T)$ with temperature suggests that $\gamma_2 \cong 1$ when T~230 K.[3] At the pressure corresponding to T = 220 K, the partial pressures calculated using these equations yields vapor phase mole fractions $y_{H2O} < 4.8\times10^{-4}$ and $y_{1\text{-prop}} < 2.1\times10^{-5}$. Comparing these values to the inlet mole fractions, we find 97% of the water and 98% of the alcohol have condensed. This yields an estimate for the average composition that is within 2% of the assumption that everything condenses.

C. Equilibration of Droplet Structure

We assume the time required to equilibrate the droplet structure is close to the time required for an alcohol molecule to diffuse from the center of a 6 nm radius droplet to the surface. In particular

$$t \approx \frac{L^2}{D} = \frac{6^2\times10^{-18}\ \mathrm{m}^2}{10^{-11}\text{ to }10^{-12}\ \mathrm{m}^2/s} < \sim 1\ \mu s. \quad \text{(S.9)}$$

Here $\underline{D}$ is the diffusion coefficient of propanol in a dilute aqueous mixture at the temperatures characteristic of the droplets when growth is essentially complete, i.e. T~230 – 250 K. At room temperature, for dilute mixtures D is on the order of 1x10^{-9} m^2/s.[4] For the purposes of this calculation, the diffusion coefficient is not that different for alcohol in water or alcohol in pure alcohol. We assume that the diffusion rate scales with temperature in a manner similar to that found in simulations of longer chain alcohols by Zangi[5] and arrive at a value of $D \sim 10^{-11} – 10^{-12}$ m^2/s and our estimate of ~ 1 μs for the diffusion time.

The simulation work of Hrahsheh *et al.*[6] that investigated the structure of binary aqueous-butanol nanodroplets (r ~ 3 nm, T = 250 K), reported that stable structures were reached well within their 100 ns simulation period whether the initial configuration was a well-mixed droplet or a core-shell structure. This suggests that our estimate for 1 μs is reasonable.

D. Droplet Temperature

As reported in our earlier work,[7, 8] once condensation slows the temperature of the droplets is very close to that of the flow. Thus, prior to the initiation of freezing the droplet temperatures are essentially equal to the flow temperature.

Once freezing starts, the model described in the SI of Amaya *et al.*[9] finds that droplets heat up to about 265 K for about 0.2 μs. To determine how this may change the average temperature of the aerosol, we need to recognize freezing is a stochastic process. Thus, only a fraction of the aerosol will be hot and the rest of the aerosol will be at the flow temperature. In Figure 14, F_{IC} increases from 0 to ~ 0.5 in ~ 40 μs. Since we argue that the system is fully frozen when F_{IC} plateaus, this suggests that in 1 μs, 1/40 = 2.5% of the aerosol freezes. Since individual droplets are only hot for ~0.2 μs, only 0.2 × 2.5% = 0.5% of the aerosol droplets are hot at any time. Thus, the "average" droplet temperature can be estimated as 0.005×265 K + 0.995×200 K = ~200.4 K. This would add a small systematic bias to the reported temperature during the rapid freezing period but is still well within our stated uncertainty of 1 K.

IV. Full FTIR Results

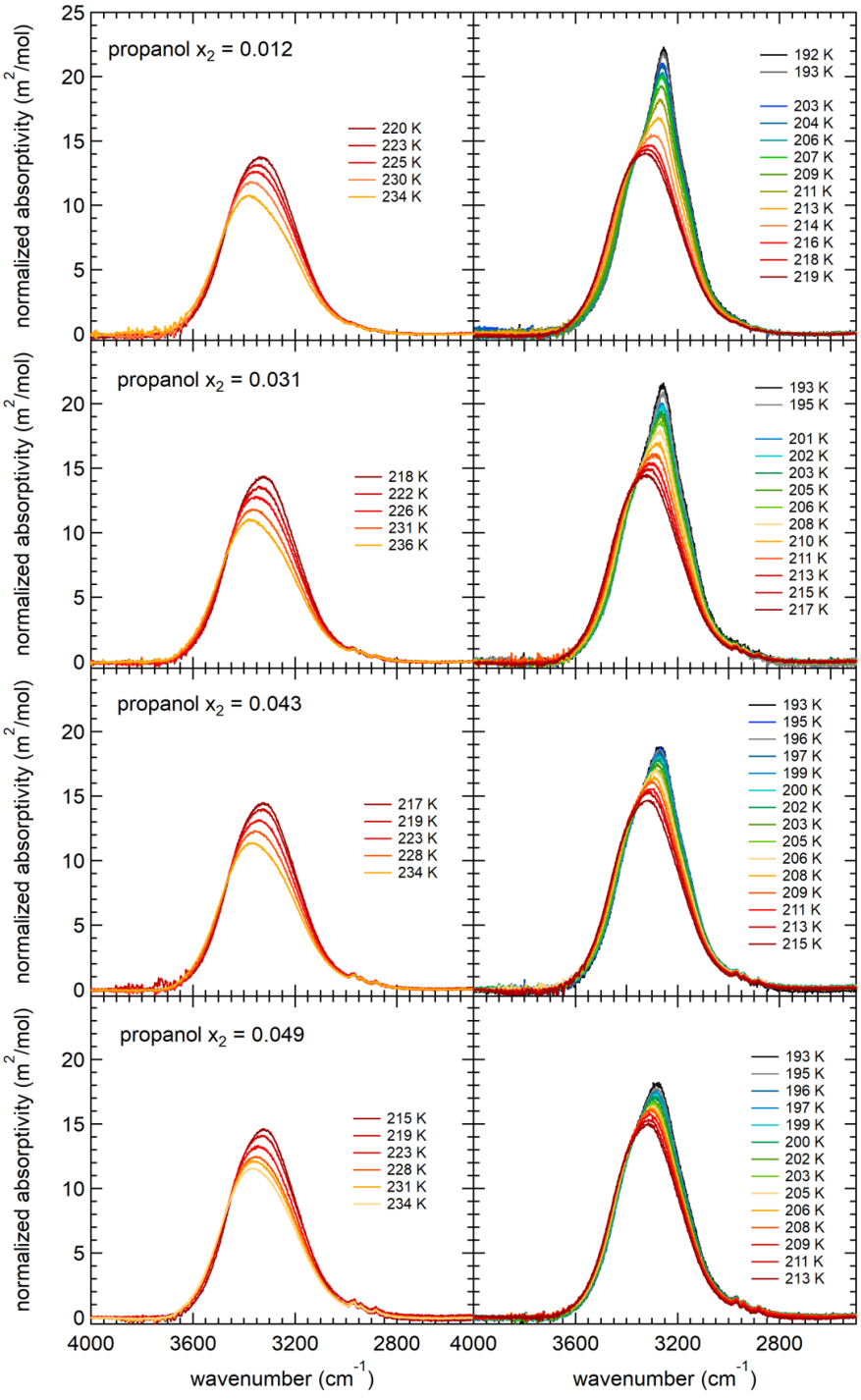

Fig. S3 IR spectra for water-propanol mixtures at the indicated mole fractions. In each pair of figures, the spectra in the left hand panel corresponds to the liquid spectra, those in the right hand panel correspond to samples transitioning to a solid state. Some spectra are not shown to enhance clarity.

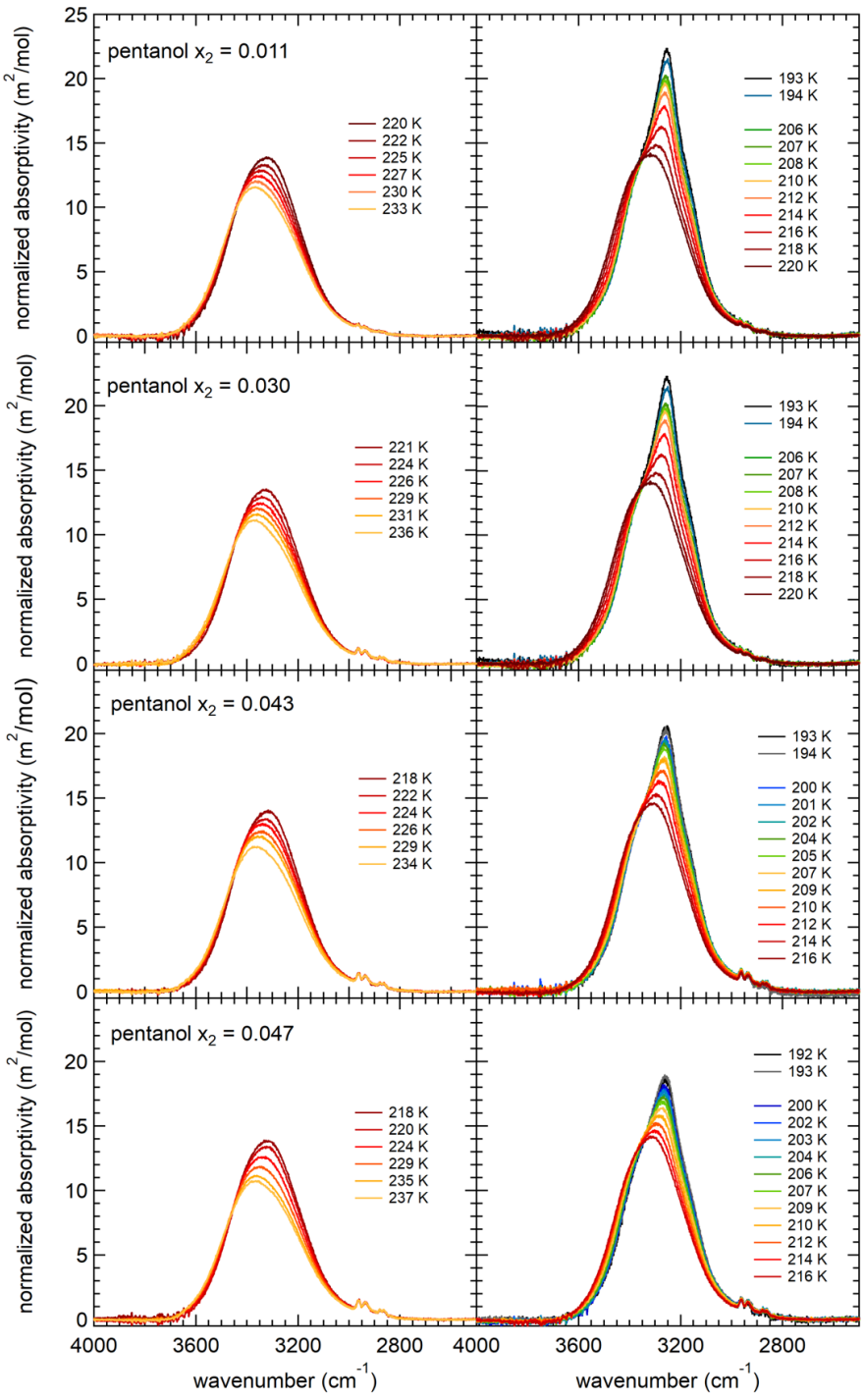

Fig. S4 IR spectra for water-pentanol mixtures at the indicated mole fractions. In each pair of figures, the spectra in the left hand panel corresponds to the liquid spectra, those in the right hand panel correspond to samples transitioning to a solid state. Some spectra are not shown to enhance clarity.

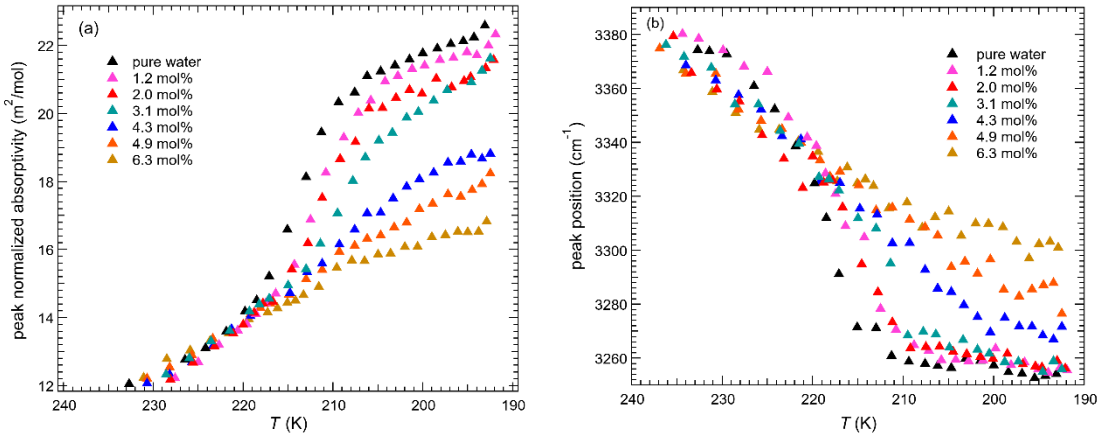

Fig. S5 The (a) peak intensity and (b) peak position for the hydrogen bonded -OH stretch band measured for the water-1-propanol aerosols vary systematically with temperature.

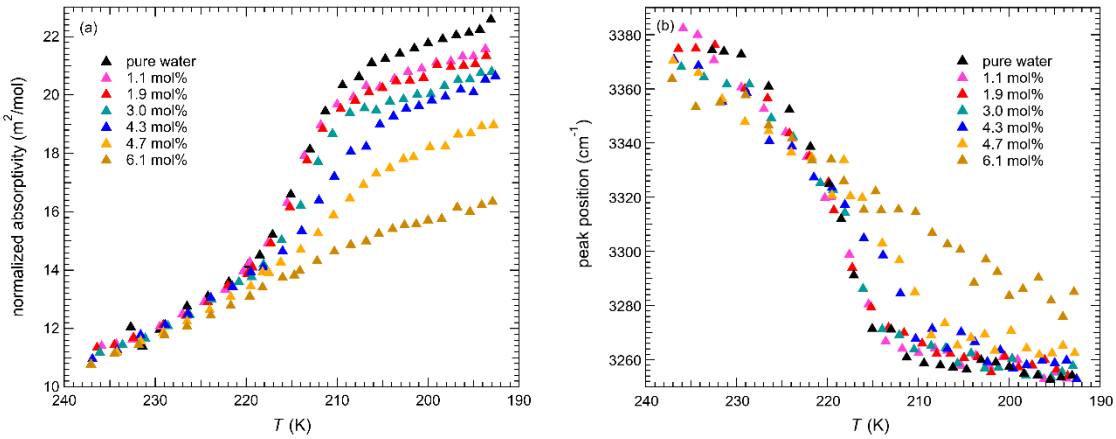

Fig. S6 (a) Peak intensity and (b) peak position for the hydrogen bonded -OH stretch band measured for the water-1-pentanol aerosols vary systematically with temperature.

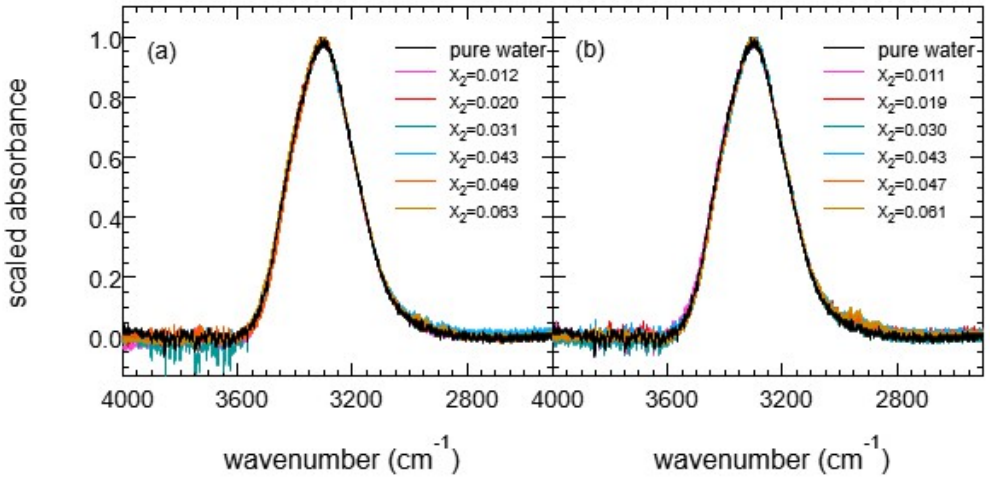

Fig. S7 Low temperature liquid component from SMCR analysis. (a) Water with propanol; (b) Water with pentanol. Peak intensity is arbitrarily scaled to 1 for easy comparison of the spectral shape.

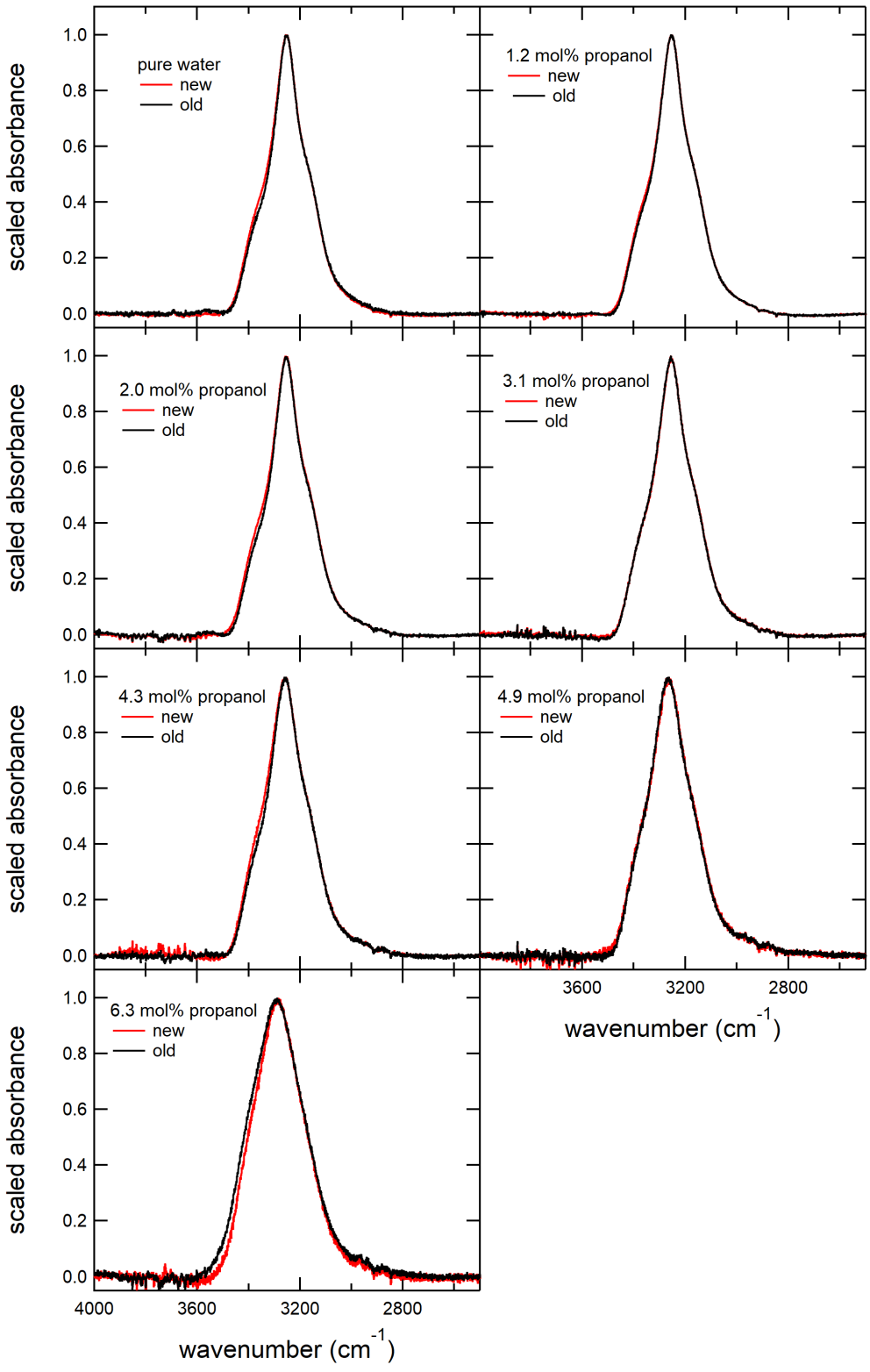

Fig. S8(a) Extracted "ice component" spectra from two independent SMCR analyses of the same propanol data sets. The temperature ranges of the first-round analyses are those indicated in Fig. S9.

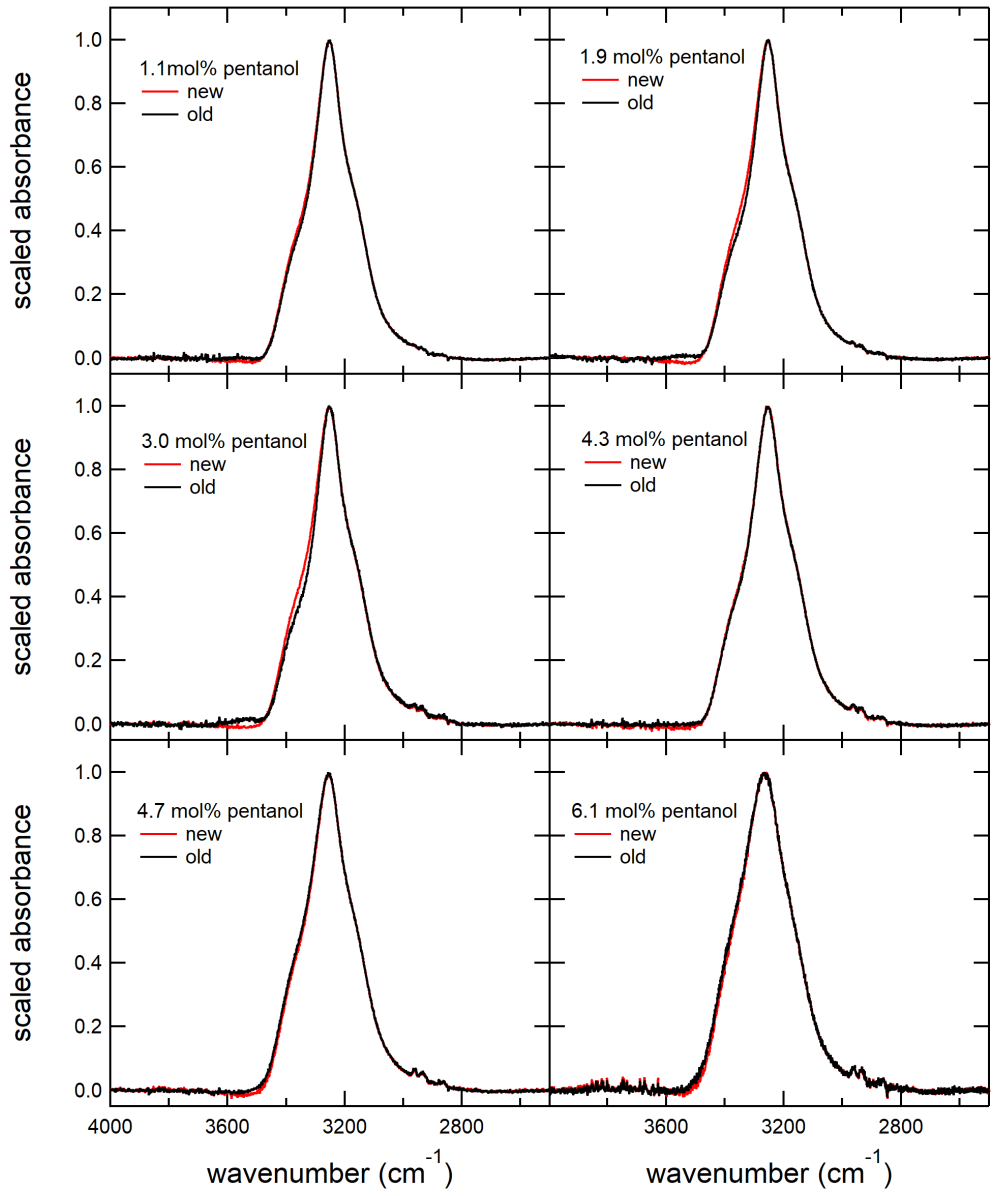

Fig. S8(b) Extracted “ice component” spectra from two independent SMCR analyses of the same pentanol data sets. The temperature ranges of the first-round analyses are those indicated in Fig. S9.

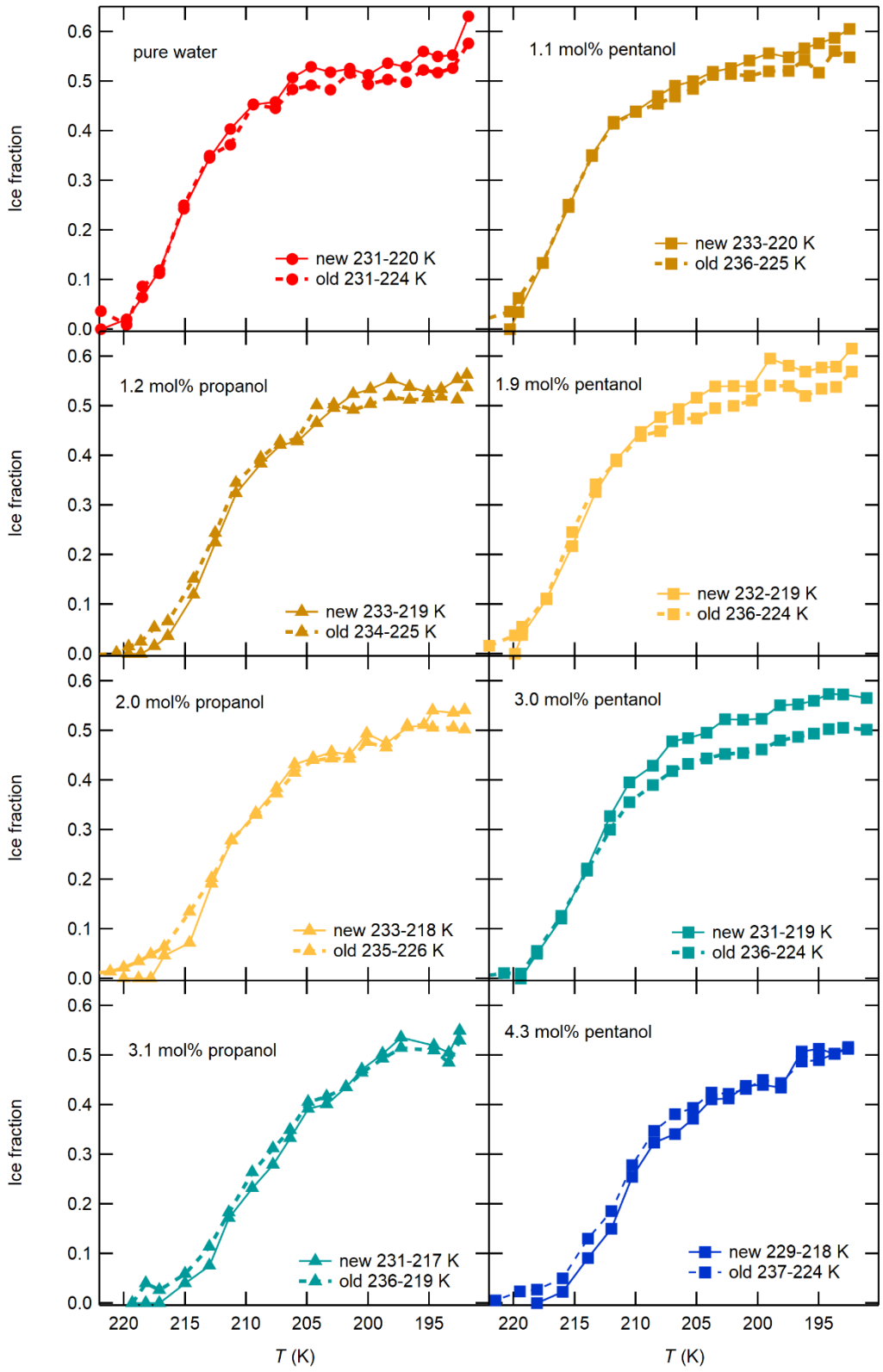

Fig. S9 Ice fraction as a function of temperature from two independent SMCR analyses, temperature ranges of spectra for the first round SMCR analysis indicated.

V. Physical Properties

A. Pure Species

Table S.1 Physical properties of the pure species

Nitrogen		Ref.
Molar mass m_{N_2} (g/mol)	28.01	
Heat capacity c_{p,N_2} (J/g K)	(28.98641+1.853978×(T/1000)-9.647459×(T/1000)^2+16.63537×(T/1000)^3+0.000117/(T/1000)^2)/28.01	Chase *et al*.[10]

H_2O		Ref.
Molar mass m_{H_2O} (g/mol)	18.02	
Heat capacity of vapor water $c_{p,H_2O(v)}$ (J/g K)	8.314× (3.9952+2.6878×10^{-4}T-2.1039×10^{-6}T^2+5.6582×10^{-9}T^3)/18.02	Tanimura *et al*.[11]

Heat capacity of liquid water $c_{\mathrm{p,H_2O}(l)}$ (J/g K)	For 231<T<285 $(75.43+2.235\times10^{-2}T- 1.749\times10^{-5}T^2+ 4.705\times10^{-8}T^3+0.1149\times\exp(0.1149\times(281.6-T)))/18.02$ For 167<T<231 $(38565.2-635.6299T+0.964611T^2 +3.646245\times10^{-2}T^3-2.189861\times10^{-4}T^4+4.197441\times10^{-8}T^5+2.456321\times10^{-9}T^6-4.839049\times10^{-12}T^7)/18.02$	Tanimura *et al.*[11]
Equilibrium vapor pressure $p_{\mathrm{eq,H_2O}}$ (Pa)	$\exp(54.842763-6763.22/T-4.210\ln T+0.000367T+\tanh(0.0415(T-218.8)) \times(53.878-1331.22/T-9.44523\ln T+0.014025T))$	Murphy and Koop [12]
Latent heat of water vaporization $H_{\mathrm{vap,H_2O}}$ (J/g)	$8.314\times(6763.22- 4.210T + 3.67\times10^{-4}T^2+ \tanh(0.0415\times(T-218.8)) \times (1331.22-9.44523T+0.014025T^2) + 0.0415/\cosh(0.0415\times(T-218.8))^2\times (53.878T^2-1331.22T - 9.44523T^2\ln(T)+1.4025\times10^{-2}T^3))/18.02$	Applying Clausius-Clapeyron equation to the equilibrium vapor pressure correlation by Murphy and Koop [12]
Water density (liquid) $\rho_{\mathrm{H_2O}}$ (g/cm^3)	$0.08\times\tanh((T-225)/46.2)+0.7415\times((T_c-T)/T_c)^{0.33}+0.320$	Wölk and Strey[13]
Surface tension $\sigma_{\mathrm{H_2O}}$ (mN/m)	$93.6635+9.133\times10^{-3}T-2.75\times10^{-4}T^2$	Viisanen *et al.*[14]
Critical temperature T_c (K)	647.15	Handbook of Chemistry and Physics[15]

1-propanol		Ref.
Molar mass m_{propanol} (g/mol)	60.10	
Heat capacity of vapor propanol $c_{\text{p,propanol}(v)}$ (J/g K)	$2.9 \times 10^{-3}T+0.538$	Data from Thermodynamics Research Center[16], fit to linear function
Heat capacity of liquid propanol $c_{\text{p,propanol}(l)}$ (J/g K)	For $185 \leq T \leq 300$ K $(-0.457965\times10^{4}+0.12403091\times10^{3}T-0.13586023\times10T^{2}+0.78792804\times10^{-2}T^{3}-0.25515782\times10^{-4}T^{4}+0.43772516\times10^{-7}T^{5}-0.3105722\times10^{-10}T^{6})/60.1$	Kalinowska *et al.*[17]
Equilibrium vapor pressure $p_{\text{eq,propanol}}$ (Pa)	$133.322\exp(84.696-8559.6/T-9.29\ln T)$	Schmeling and Strey[18]
Latent heat of propanol vaporization $H_{\text{vap,propanol}}$ (J/g)	$8.314\times(8559.6-9.29T)/60.1$	Applying Clausius-Clapeyron equation to the equilibrium vapor pressure correlation by Schmeling and Strey[18]
Propanol density (liquid) ρ_{propanol} (g/cm^3)	$(1010.77-3.99649\times10^{-5}T-6.64293\times10^{-3}T^{2}+2.16751\times10^{-5}T^{3}-2.46167\times10^{-8}T^{4}/1000$	Frenkel *et al.*[19]

Surface tension σ_{propanol} (mN/m)	25.28-8.394×10^{-2}(T-273.15)	Strey and Schmeling[20]

1-pentanol		Ref.
Molar mass m_{pentanol} (g/mol)	88.15	
Heat capacity of the vapor pentanol $c_{\text{p,pentanol}(v)}$ (J/g K)	8.22×(1.73+8.2×10^{-3}T) ×4.184/88.15	Stromsoe *et al.*[21]
Heat capacity of the liquid pentanol $c_{\text{p,pentanol}(l)}$ (J/g K)	For 195.56≤T≤390 5.5423-4.2546×10^{-2}T+1.4888×10^{-4}T^2-1.4×10^{-7}T^3	Data from Counsell *et al.*[22], fit to polymonial
Equilibrium vapor pressure $p_{\text{eq,pentanol}}$ (Pa)	133.322exp(90.08-9788.4/T-9.9ln$T$)	Schmeling and Strey[18]
Latent heat of pentanol vaporization $H_{\text{vap,pentanol}}$ (J/g)	8.314×(9788.4-9.9T)/88.15	Applying Clausius-Clapeyron equation to the equilibrium vapor pressure correlation by Schmeling and Strey[18]

Pentanol density (liquid) $\rho_{pentanol}$ (g/cm^3)	(1100.3-1.58026T+3.34384×10$^{-3}T^2$-4.34342×10$^{-6}T^3$)/1000	Frenkel *et al.*[19]
Surface tension $\sigma_{pentanol}$ (mN/m)	26.78-8.147×10^{-2}(T-273.15)	Strey and Schmeling[20]

*The unit of T is Kelvin (K).

In the experimental temperature range, the equilibrium vapor pressures of the normal alcohols are lower than that of water and decrease as the chain length increases. Relevant data are plot in Fig. S10.

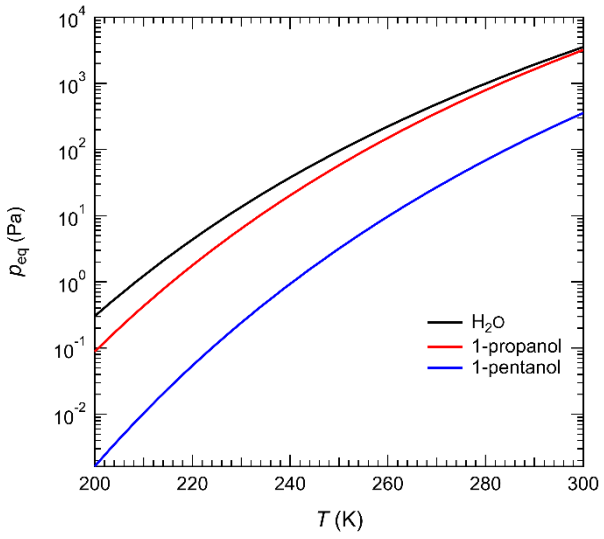

Fig. S10 Vapor pressure of water[12], 1-propanol and 1-pentanol.[18]

B. Mixture Properties

The mixture properties of interest include mutual solubility, density and surface tension.

1. Water-1-propanol

Propanol water mixtures are miscible over the composition full range.

Since the mixtures are non-ideal systems, the density of aqueous-propanol solution deviates from the linear combination of the two components. Zarei and Shahvarpour measured the excess molar volume through the entire composition range for water-propanol system from 293.15 K to 323.15 K.[23] The density at 293.15 K is shown in Fig. S11. Assuming the system is ideal, the blue curve is calculated by

$$\rho = \frac{x_1 m_1 + x_2 m_2}{x_1 v_1 + x_2 v_2}, \tag{S.10}$$

where m is the molar mass of pure component and v is the molar volume which can be derived from density stated in Table S1. The orange curve is calculated by

$$\rho = \frac{x_1 m_1 + x_2 m_2}{v + v^E}, \tag{S.11}$$

where $v = \frac{x_1 m_1}{\rho_1} + \frac{x_2 m_2}{\rho_2}$ and v^E is the excess molar volume at each composition given by Zarei and Shahvarpour. The grey curve comes from the measured densities of Zarei and Shahvarpour. The orange and grey lines ones overlap nicely while they deviate from the ideal mixture at the intermediate mole fractions. Density deviation from the ideal situation

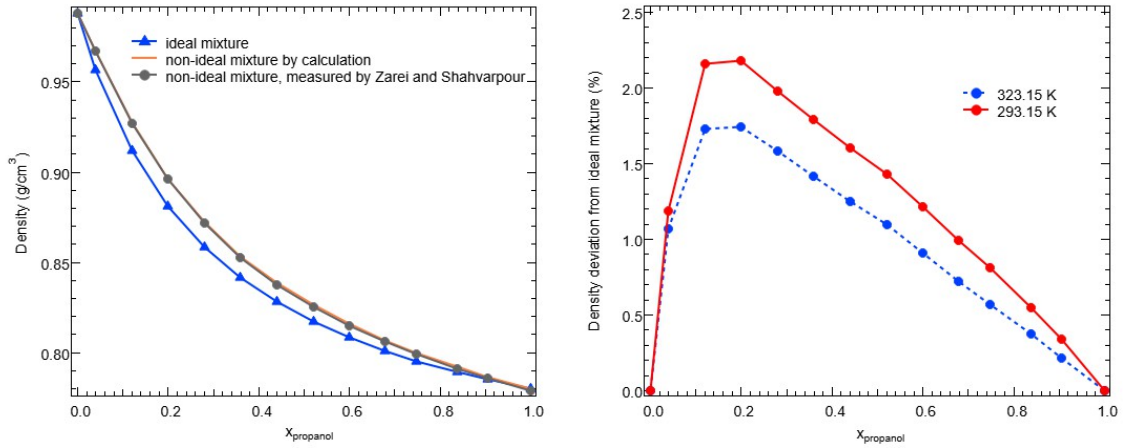

Fig. S11 Left: Density profiles for water-propanol as a function of propanol mole fraction. Ideal mixture (blue curve); non-ideal mixture by calculation, using density data of pure component from Table S1 and excess molar volume from Zarei and Shahvarpour (orange curve); Right: Non-ideal mixture density measured by Zarei and Shahvarpour.

$$\Delta\rho = \frac{\rho_{\text{non-ideal}} - \rho_{\text{ideal}}}{\rho_{\text{ideal}}} \times 100\% \qquad \text{(S.12)}$$

is plot against mole fraction at 293.15 K and 323.15 K, where $\rho_{\text{non-ideal}}$ refers to the calculated density of non-ideal mixture. The maximum deviation occurs at x_{propanol}=0.2 for both temperatures and $\Delta\rho$ increases ~0.44% as temperature decreases 30 K. The deviation is ~1.1% if it is extrapolated to 220 K, which should be safe to ignore the nonideality.

Since the surface tension of an aqueous-alcohol solution is not a linear function of solute mole fraction, experimental data from the published literature are analyzed and extrapolated.[1] At each propanol concentration, the surface tension data between 20 and 50 °C are fit to a linear function of temperature and extrapolated to lower temperatures, see Fig. S12. Because the mole fractions of propanol (x_2) in the current study range from ~0.01 to ~0.08, only the data for x_2=0.016-0.091 are used to ensure good accuracy of fitting within the concentration range of interest.

The extrapolated data are then fit to the Szyszkowski equation

$$\sigma(T) = \sigma_{\text{H}_2\text{O}}(T) - A\ln(1 + \frac{C_{\text{b}}}{B}), \qquad \text{(S.13)}$$

where $\sigma_{\text{H}_2\text{O}}$ is water surface tension and C_{b} is the molarity of the solute in the bulk phase or total molarity M in the bulk system.[24] Here M is calculated as

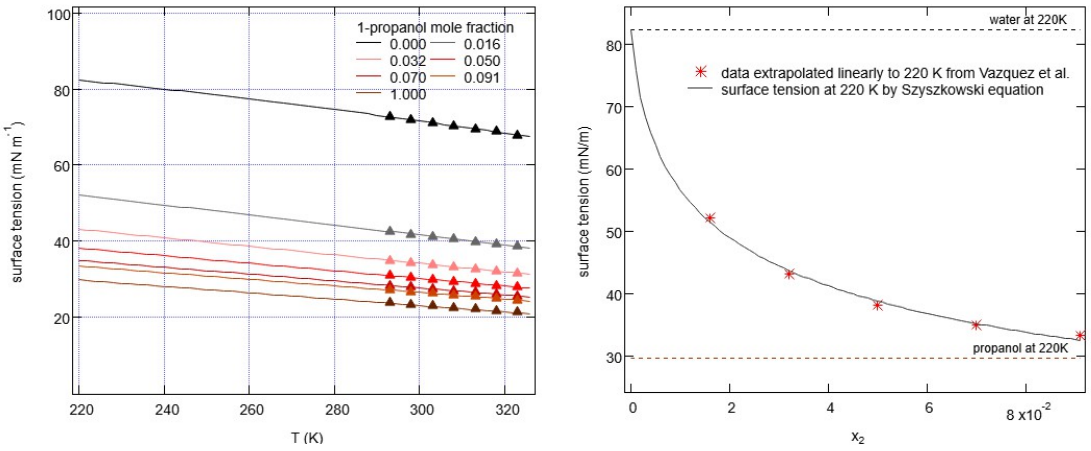

Fig. S12 Left: Surface tension of aqueous-1-propanol. Triangles from Vazquez *et al*. Lines: pure water is from Wölk and Strey, aqueous-1-propanol solutions are linear fitting of data from Vazquez *et al*., pure propanol is from Strey and Schmeling. Right: Surface tension of aqueous-1-propanol at 220 K, linearly extrapolated from Vazquez *et al*. (red asterisk); Trend given by fitting data of Vazquez *et al*. and pure water from Wölk and Strey to the Szyszkowski equation (black line). Water at 220 K is from Wölk and Strey (dashed black line); propanol at 220 K is from Strey and Schmeling (dashed crimson line).

$$M = \frac{\rho x_2}{(m_{\text{propanol}} - m_{\text{H2O}})x_2 + m_{\text{H2O}}}, \quad \text{(S.14)}$$

where ρ is the solution density at relevant temperatures, calculated by Eq (S.10). The resultant parameters are A =12.75, B = 0.07949 at 220 K, as shown in Fig. S12.

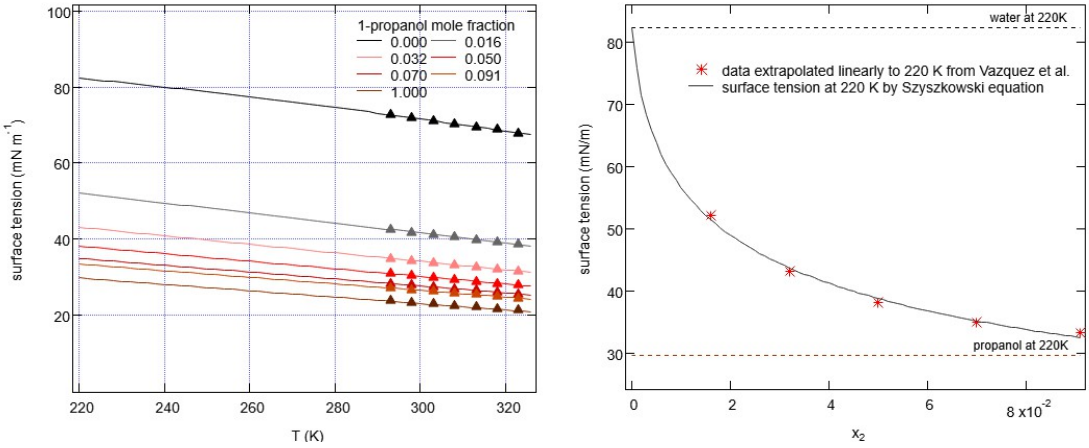

Fig. S12 Left: Surface tension of aqueous-1-propanol. Triangles from Vazquez *et al*. Lines: pure water is from Wölk and Strey, aqueous-1-propanol solutions are linear fitting of data from Vazquez *et al*., pure propanol is from Strey and Schmeling. Right: Surface tension of aqueous-1-propanol at 220 K, linearly extrapolated from Vazquez *et al*. (red asterisk); Trend given by fitting data of Vazquez *et al*. and pure water from Wölk and Strey to the Szyszkowski equation (black line). Water at 220 K is from Wölk and Strey (dashed black line); propanol at 220 K is from Strey and Schmeling (dashed crimson line).

2. Water-1-pentanol

1-pentanol and water mixtures exhibit a solubility gap that is temperature dependent. The solubility data are, however, only available for near or above room temperature for both water-rich and pentanol-rich phase. The extrapolation of pentanol solubility in water-rich phase by the empirical equation proposed by Goral *et al*.[25] suggests a rapid increase in pentanol solubility in water as temperature decreases down to 200 K, as shown in Fig. S13. At ~220 K, x_2=0.058, which should be well above the calculated bulk mole fractions of the droplets in this study. The solubility of water in pentanol-rich phase is also plotted to show the conceivable miscibility gap.[25, 26]

Density of water-pentanol systems is only available for very dilute conditions. According to Pai and Chen[27], the density is 0.99548 g/cm^3 when x_{pentanol}=0.0036 at 293.15K, increased by 0.12% compared to the ideal case. Here the nonideality of aqueous-pentanol solution is also ignored in the model calculation.

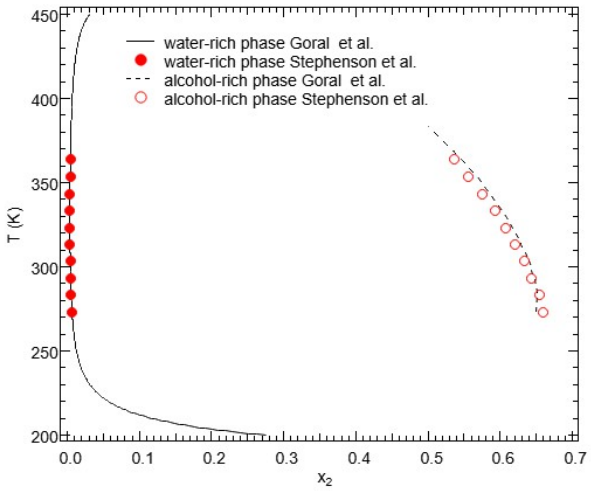

Fig. S13 Solubility of water-1-pentanol solution. Data extracted from Goral *et al*.[25] and Stephenson *et al*. [26]

Surface tension data for the water-1-pentanol system is only available for mole fractions up to x_2 =0.003103 due to the limited solubility of pentanol in water.[2] In our model calculation, however, the calculated bulk mole fraction is well below this limit, so that it is safe to use the data and fit them into Szyszkowski equation. The parameters for water-pentanol is A = 16.22, B = 9.3023×10^{-3}. Relevant data are present in Fig S14.

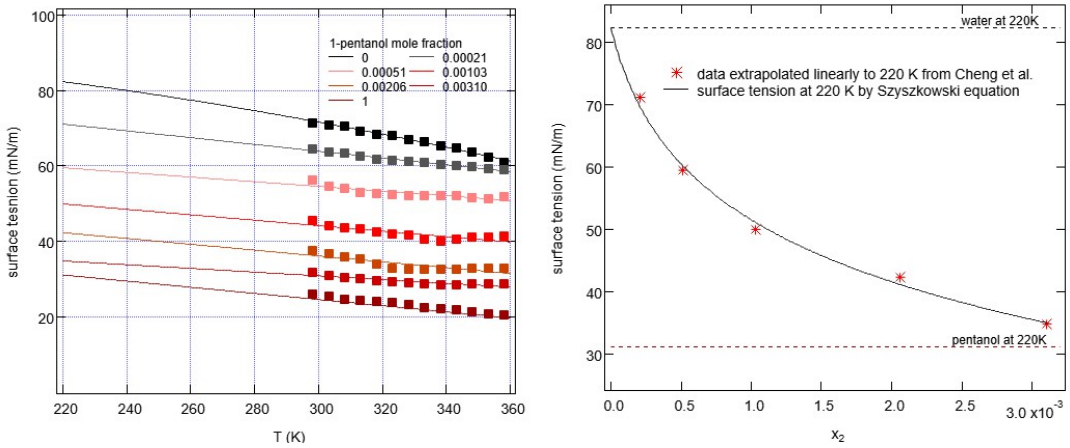

Fig. S14 Left: Surface tension of aqueous-1-pentanol. Triangles from Cheng *et al.* Lines: pure water is from Wölk and Strey, aqueous-1-pentanol solutions are linear fitting of data from Cheng *et al*., pure pentanol is from Strey and Schmeling. Right: Surface tension of aqueous-1-pentanol at 220 K, linearly extrapolated from Cheng *et al*. (red asterisk); Trend given by fitting data of Cheng *et al*. and pure water from Wölk and Strey to the Szyszkowski equation (black line). Water at 220 K is from Wölk and Strey (dashed black line); pentanol at 220 K is from Strey and Schmeling (dashed crimson line).

VI. Particles Size Measurements

The particle size given in Section III. A was measured by Small angel x-ray scattering for pure water and water-1-pentanol systems with the initial condition p_{0,H_2O} = 1.05 kPa in the same nozzle,[28] as shown in Fig. S15.

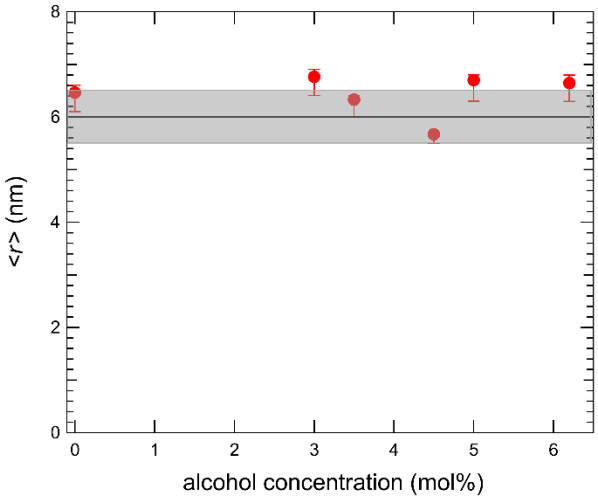

Fig. S15 Particle radius range for pure water and water-1-pentanol mixtures. Error bars show the upper and lower limit of the particle size from 4.5 cm downstream of the throat to the nozzle end. The shaded area reflects particle size used in the main text, i.e. 6 ± 0.5 nm.

References

1. G. Vazquez, E. Alvarez and J. M. Navaza, *Journal of Chemical and Engineering Data*, 1995, **40**, 611-614.
2. K. K. Cheng and C. Park, *Heat and Mass Transfer*, 2017, **53**, 2255-2263.
3. V. Dohnal, D. Fenclova and P. Vrbka, *Journal of Physical and Chemical Reference Data*, 2006, **35**, 1621-1651.
4. K. C. Pratt and W. A. Wakeham, *Proceedings of the Royal Society of London. A. Mathematical and Physical Sciences*, 1975, **342**, 401-419.
5. R. N. Zangi, *Acs Omega*, 2018, **3**, 18089-18099.
6. F. Hrahsheh, Y. S. Wudil and G. Wilemski, *Physical Chemistry Chemical Physics*, 2017, **19**, 26839-26845.
7. H. Pathak, K. Mullick, S. Tanimura and B. E. Wyslouzil, *Aerosol Science and Technology*, 2013, **47**, 1310-1324.
8. Y. Park, S. Tanimura and B. E. Wyslouzil, *Aerosol Science and Technology*, 2016, **50**, 773-780.
9. A. J. Amaya, H. Pathak, V. P. Modak, H. Laksmono, N. D. Loh, A. S. Jonas, R. G. Sierra, T. A. McQueen, M. J. Hayes, G. J. Williams, M. Messerschmidt, S. Boutet, M. J. Bogan, A. Nilsson, C. A. Stan and B. E. Wyslouzil, *Journal of Physical Chemistry Letters*, 2017, **8**, 3216-3222.
10. M. W. Chase, Jr., *NIST-JANAF Themochemical Tables, Fourth Edition*, fourth edition edn., 1998.
11. S. Tanimura, B. E. Wyslouzil and G. Wilemski, *Journal of Chemical Physics*, 2010, **132**, 144301.
12. D. M. Murphy and T. Koop, *Quarterly Journal of the Royal Meteorological Society*, 2005, **131**, 1539-1565.
13. J. Wolk and R. Strey, *Journal of Physical Chemistry B*, 2001, **105**, 11683-11701.
14. Y. Viisanen, R. Strey and H. Reiss, *Journal of Chemical Physics*, 1993, **99**, 4680-4692.
15. *Handbook of Chemistry and Physics*, CRC Press, Boca Raton, 84th edn., 2003.
16. *Selected Values of Properties of Chemical Compounds*, Thermodynamics Research Center, Texas A&M University, 1997.
17. B. Kalinowska, J. Jedlinska, W. Woycicki and J. Stecki, *Journal of Chemical Thermodynamics*, 1980, **12**, 891-896.
18. T. Schmeling and R. Strey, *Berichte Der Bunsen-Gesellschaft-Physical Chemistry Chemical Physics*, 1983, **87**, 871-874.
19. M. Frenkel, X. Hong, R. C. Wilhoit and K. R. Hall, *Densities of Alcohols*, Landolt-Börnstein 2000.
20. R. Strey and T. Schmeling, *Berichte Der Bunsen-Gesellschaft-Physical Chemistry Chemical Physics*, 1983, **87**, 324-327.

21. E. Stromsoe, H. G. Ronne and A. L. Lydersen, *Journal of Chemical and Engineering Data*, 1970, **15**, 286-290.
22. J. F. Counsell, E. B. Lees and J. F. Martin, *Journal of the Chemical Society a -Inorganic Physical Theoretical*, 1968, 1819-1823.
23. H. A. Zarei and S. Shahvarpour, *Journal of Chemical and Engineering Data*, 2008, **53**, 1660-1668.
24. J. Malila and N. L. Prisle, *Journal of Advances in Modeling Earth Systems*, 2018, **10**, 3233-3251.
25. M. Goral, B. Wisniewska-Goclowska and A. Maczynski, *Journal of Physical and Chemical Reference Data*, 2006, **35**, 1391-1414.
26. R. Stephenson, J. Stuart and M. Tabak, *Journal of Chemical and Engineering Data*, 1984, **29**, 287-290.
27. Y. H. Pai and L. J. Chen, *Journal of Chemical and Engineering Data*, 1998, **43**, 665-667.
28. A. J. Amaya, PhD, The Ohio State University, 2018.